Chemical Physics Letters 826 (2023) 140649

Contents lists available at ScienceDirect

Chemical Physics Letters

journal homepage: www.elsevier.com/locate/cplett

Research paper

First-principles calculations of the AlN/Ti interface properties

Lei Li [a], Xueyan Yan [a], Bingzheng Yang [a], Sen Yang [a], Alex A. Volinsky [c], Xiaolu Pang [a,b,*]

[a] School of Materials Science and Engineering, University of Science and Technology Beijing, Beijing 100083, China
[b] State Key Laboratory of Nuclear Power Safety Technology and Equipments, School of Mathematics and Physics, University of Science and Technology Beijing, Beijing 100083, China
[c] Department of Mechanical Engineering, University of South Florida, 4202 E. Fowler Ave. ENG030, Tampa 33620, USA

ARTICLE INFO

Keywords:
First-principles calculations
Interface
Thermal stability
Orientation

ABSTRACT

AlN substrates are widely used in power modules and have high thermal conductivity and good insulation performance. In order to study the thermal stability of AlN substrates coated with the active metal, the AlN/Ti interface structure and the temperature dependence of the AlN layer orientation were investigated using the first principles calculations. The calculated work of separation and distance at elevated temperatures demonstrated good thermal stability of the interface. Elastic and shear modulus were calculated for the interface elastic anisotropy analysis and a certain orientation dependence was found. This study is helpful for the development of novel high-power microelectronic devices.

1. Introduction

With the integration and miniaturization of electronic devices, ceramic substrates have been widely used for structural support and heat dissipation at high temperatures in high-power modules such as insulated gate bipolar transistors, and light-emitting diodes [1,2]. The third generation wide band gap semiconductor materials like gallium nitride (GaN) and silicon carbide (SiC), have been used in novel high-power devices with higher breakdown voltage, lower switching losses, and higher carrier density, theoretically withstanding up to 600 °C [3]. Therefore, the primary concern when choosing electronic packing materials is the delamination failure resulting from severe thermal strain and shock.

Direct-plated copper (DPC) and direct-bonded copper are promising techniques for printed circuit board manufacturing. Ceramics with high thermal conductivity, low coefficient of thermal expansion (CTE), and excellent thermal resistance can serve as DPC electronic packing substrates. The aluminum nitride AlN substrates have excellent thermal conductivity k = 180–260 W/mK compared with other ceramic substrates such as Al2O3 with k = 30 W/mK, and thus demonstrate more efficient heat dissipation [4]. Besides heat dissipation, the thermal reliability of high-power modules under high-temperature cycling induced by CTE mismatch between metal and ceramic substrates remains a problem for DPC electronic packing [5]. Therefore, to eliminate delamination failure resulting from thermal shock, it is crucial to maintain a strongly bonded interface resulting in high reliability of the metal-ceramic layers. The effect of temperature on the crystal stability and mechanical properties of materials can be studied by first-principles calculations. For example, Diao et al. studied the possible decomposition mechanism of perovskite materials at different temperatures by DFT [6], and Wang et al. found that the elastic constants (C_{ij}), mechanical moduli (B, G, E) and Poisson's ratio (ν) of Ir_3Nb decreased with increasing temperature [7]. Moreover, DFT computation of metal nitrides' stacking fault energy (SFE) revealed that temperature elevation reduced the SFE [8]. When ceramic and metal layers were applied to thermal stress and external stress, it is crucial to build a strong bonded interface with high thermal reliability and high stress-resistance. As elastic constants give the response of the crystal to external forces and thus play an important role in determining the strength, ductility, and hardness of materials, anisotropic elastic properties should be addressed when suffering from different direction loading.

Theoretical and experimental studies suggested that high-strength bonded interfaces between AlN and metals improve their thermal shock resistance. Therefore, previous studies have focused on the atomic structure and the nature of ceramic/metal interface bonding. Cai et al. [9] investigated properties and bonding energy between the deposited palladium, silver, copper, and the clean Al-terminated (0001) surface of wurtzite AlN using the density-functional theory. Hybridization of deposited Pd results in the higher bonding energy of the Pd/AlN interface. Also, Al, Cu, Ti, and Zr with AlN interfaces were constructed in the

* Corresponding author at: School of Materials Science and Engineering, University of Science and Technology Beijing, Beijing 100083, China.
E-mail address: pangxl@mater.ustb.edu.cn (X. Pang).

https://doi.org/10.1016/j.cplett.2023.140649
Received 24 February 2023; Received in revised form 17 May 2023; Accepted 6 June 2023
Available online 10 June 2023

study of Tao et al. [10]. Mathematical models and density functional theory demonstrated that adhesion strength is directly related to the lattice mismatch, and does not have a direct relationship with either formation enthalpy or the surface energy. Our previous study found that Ti (0001) has stronger Np orbital hybridization and lower Ti-N bond length than Cr (1 1 0) for AlN (0001) substrate [11].

Moreover, residual stress generated by thermal shock affects the ceramic/metal interface performance significantly. Excessive residual stress can lead to warping and cracking [12,13], which compromises the reliability of the ceramic substrate and poses a major challenge for developing and applying related devices [14]. Hence, investigating the interface mechanical energy at various temperatures can assess its deformation capacity during heating and cooling, which is crucial for enhancing the precision and service performance [15].

According to our previous research on the AlN (0001)/Ti (0001) interface, the N-terminal interface with TL stacking sequences exhibits larger Wsep and shorter d0 compared to other structures [16]. TL stacking at the N-terminal interface shows the mixing of covalent bond and ionic bond. In this work, the structure of the interface between the AlN layer and Ti substrate was considered. The Helmholtz free energy and thermal volume expansion of AlN and Ti were computed and an interface structure of the ground state was built to study the thermal stability of the interface. To estimate the elastic anisotropy of the interface structure, elastic and shear moduli were calculated and an orientation dependence was found.

2. Computational methods

2.1. Thermodynamics methods

Equilibrium lattice properties at a finite temperature of AlN and Ti have been investigated using quasi-harmonic approximation (QHA) which states that phonon frequencies become volume-dependent [9]. The Helmholtz free energy in QHA is expressed as

$$F^{QHA}(T,V) = E_{stat}(V) + F_{vib}^{QHA}(T,V) - TS(T,V) \tag{1}$$

Here, the first part $E_{stat}(V)$ is the static energy of total systems at $T = 0$ K, and the second part $F_{vib}^{QHA}(T,V)$ is introduced as phonon contribution of the anharmonic effect

$$F_{vib}^{QHA}(T,V) = k_B T \sum_{i,q}\left[\frac{\hbar\omega_{i,q}(V)}{2k_BT} + \ln\left(1 - e^{-\frac{\hbar\omega_{i,q}(V)}{k_BT}}\right)\right] \tag{2}$$

Here, $\omega_{i,q}(V)$ is the phonon frequency at which q is the wave vector and i is the band index [9]. Therefore, entropy S at constant volume and heat capacity C_V could be calculated as

$$S(T,V) = k_B\left[\sum_{i,q}\frac{\hbar\omega_{i,q}(V)}{k_BT\left(e^{\frac{\hbar\omega_{i,q}(V)}{k_BT}} - 1\right)} - \sum_{i,q}\ln\left(1 - e^{-\frac{\hbar\omega_{i,q}(V)}{k_BT}}\right)\right] \tag{3}$$

$$C_V = \sum_{i,q} k_B\left(\frac{\hbar\omega_{i,q}(V)}{k_BT}\right)^2 \frac{\exp\left(\frac{\hbar\omega_{i,q}(V)}{k_BT}\right)}{\left[\exp\left(\frac{\hbar\omega_{i,q}(V)}{k_BT}\right) - 1\right]^2} \tag{4}$$

In addition, the heat capacity under a constant pressure C_P is derived from the $S(T,V)$ [10]

$$\begin{aligned} C_P &= T\left(\frac{\partial S(T,V)}{\partial T}\right)_P = T\left(\frac{\partial S}{\partial T}\right)_V + T\left(\frac{\partial S}{\partial V}\right)_T\left(\frac{\partial V}{\partial T}\right)_P \\ &= C_V + \alpha_V VT\left(\frac{\partial S}{\partial V}\right)_{V=V(T,P)} \end{aligned} \tag{5}$$

Here, α_V is the volume thermal expansion coefficient.

2.2. Computational details

Structure optimization and theoretical ground state mechanical properties of AlN and Ti under the framework of density functional theory were calculated by Vienna Ab initio simulation package code [17,18] with projector augmented plane wave [19]. This study chose Erdew-Burke-Ernzerhof's generalized gradient approximation [20] to describe the exchange–correlation energy. For the Brillouin zones, gamma-centered Monkhorst-Pack k-point was sampled with a mesh grid of 9 × 9 × 9, 9 × 9 × 1 and 9 × 9 × 1 for the bulk AlN, surface, and interface, respectively. The plane wave cutoff energy was set to 400 eV for the convergence tests. Relaxation of atomic structure was achieved by utilizing the Quasi-Newton RMM-DIIS algorithm. The convergence criterion of minimization force per atom was reduced to 0.02 eV/Å and total energy was minimized until convergence within 10E-5 eV.

Thermodynamic properties such as heat capacity at constant volume C_V, entropy S, and thermal expansion coefficient α_V were all derived from the Helmholtz energy at various elevated temperatures. Thirteen volume points with a maximum volume variation of less than l5% around equilibrium were calculated at each temperature range, and equilibrium volumes at different temperatures were fitted using the equation of state [21]. Temperature dependencies of elastic constants were obtained using the strain–stress relationship methods by Milman et al. [22]. Tensile and compressed states were all simulated with a maximum strain within the 0.2% convergence criteria of atomic structure optimization. Bulk modulus B, shear modulus G, and elastic modulus E ranged with temperature and were calculated by using the Voigt-Reuss-Hill approximation [23,24].

3. Results and discussion

3.1. Ground state structure

Previous studies suggested that the wurtzite structure was preferred to the rock salt structure for AlN [25,26]. The lattice parameters calculated in this study were a = b = 3.128 Å, c = 5.016 Å, which are comparable with the experimental data: a = b = 3.126 Å, c = 5.008 Å [27]. The optimized hexagonal structure of α-Ti with calculated lattice constants a = b = 2.955 Å, c = 4.664 Å is the similar to previously reported experimental data [28].

3.2. Thermodynamic properties

The equation of state (EOS) is composed of the function of states, such as temperature (T), pressure (P), volume (V), and internal energy or specific heat. It characterizes the atomic structure, chemical bonding, and stability of a material. Volume-dependent Helmholtz free energy of AlN and Ti at various temperatures was calculated using the QHA method with the results shown in Fig. 1.

According to Fig. 1, ascending temperature gives rise to equilibrium volume. The volume expansion of AlN from 0 K to 900 K is around 1.11%, while Ti volume expansion is around 2.29%. These minor volume changes in the bulk materials show the thermal stability of the crystal structure. Volume expansion $\Delta V/V_0$, where V_0 is the volume at 300 K, is plotted in Fig. 2. In the inset graph of Fig. 2, linear volume expansion starts at higher temperatures past 500 K like in other III-nitrides (GaN and InN), which shows unchanged intrinsic phonon energy of a typical solid system bellow 110 K [29]. As for Ti, volume expansion changes rapidly above 60 K.

To estimate the stability of the interface structure at extreme temperatures, the electronic structure and interface energy of the AlN/Ti interface have been explored. Previous work suggested that among the different orientations of AlN/Ti, different atomic termination and stacking sequences attributed to different work of separation. AlN (0001)/Ti(0001) with Al-terminated and OL stacking sequence exhibited the highest work of separation and was also chosen in this study for

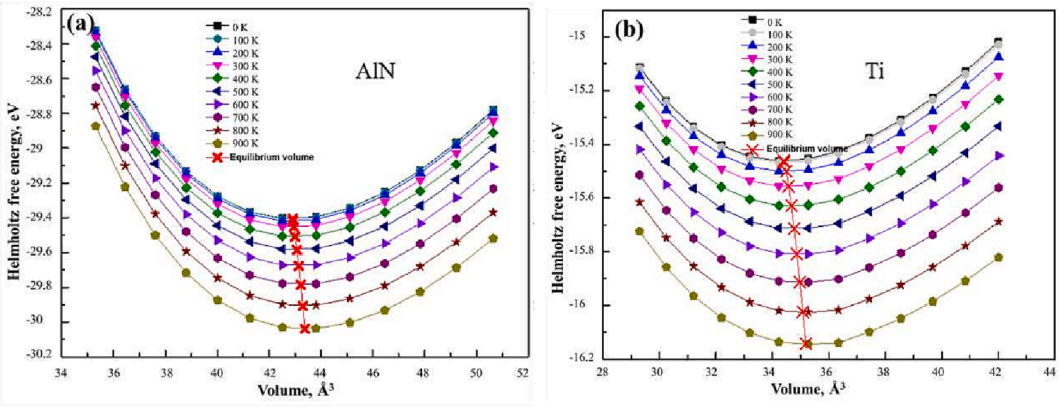

Fig. 1. Volume-dependent Helmholtz free energy of AlN and Ti. Solid lines demonstrate fitting curves using Vinet's EOS and the red line with crosses highlights the minimum volume values at elevated temperature: (a) AlN; (b) Ti.

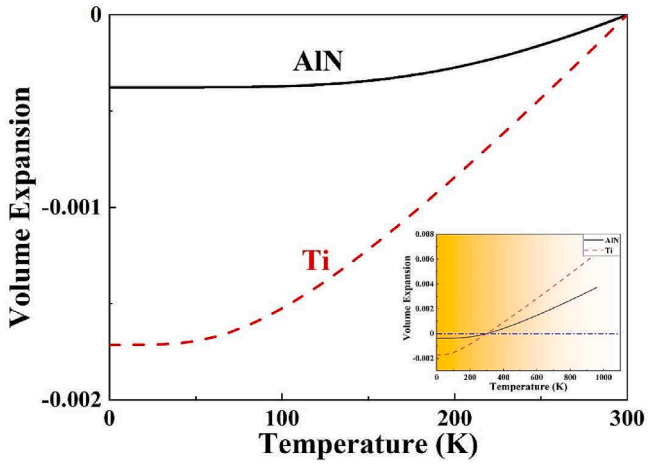

Fig. 2. Volume expansion of AlN and Ti from 0 K to 1,000 K.

thermal properties calculations. The detailed interface structure is shown in Fig. 3.

As the temperature increases, the lattice parameters have a minor change, so the orientation and interface distance keep still compared to the ground state. After geometry optimization, interface distance and work of separation at all temperatures have been calculated, listed in Table 1. From 0 K to 700 K, the interface distance is nearly unchanged, and the work of separation also tends to decrease. The minor decrease in the work of separation and the negligible change in the interface distance imply the stability of the interfacial structure at high temperatures.

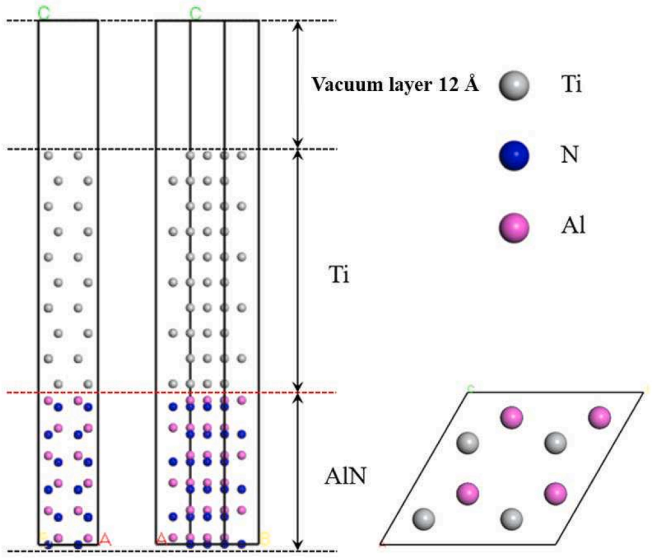

Fig. 3. Ground state AlN(0001)/Ti(0001) interface structure.

The work of separation denotes the ceramic/metal interface bond strength. The atomic orbital hybridization and electron transition near the surface control the structural stability of the surface. In the research of Zhang et al. [11], hybridized Ti-spd and N-p orbitals had strong covalent character and showed higher interfacial energy compared with the AlN/Cr interface. Therefore, the covalent bonds between Ti and N atoms are Ti-spd and N-p orbital hybridization.

The phonon density of the AlN/Ti interface was also constructed to analyze the lattice vibration of the interfacial system in all temperature ranges. Lattice vibrations are strongly influenced by the heat input. Fig. 4 shows that the total density of states is lower, and the contribution of the high-frequency region (15–25 THz) becomes larger at higher temperatures.

To explore the lattice vibrations of AlN and Ti in the studied temperature range, the thermal expansion coefficients and Grüneisen parameters have also been considered. Applying quasi-harmonic approximation to characterize the volume-depend atomic vibrations, the anharmonicity of interatomic vibrations induces the thermal expansion and Grüneisen parameter to show the temperature effects. The Grüneisen parameter is

$$\gamma_{i,q} = \frac{dln\omega_{i,q}}{dlnV} \tag{6}$$

Here, i is the mode number, q is the wave vector, and $\gamma_{i,q}$ is a measure of the anharmonicity of the whole system. Since the thermal expansion is without pressure, the C_V can be introduced using Talyor expansion around the equilibrium volume point:

$$K\frac{1}{V_0}\left(\frac{\partial V}{\partial T}\right)_P = \gamma\frac{V\left(\frac{\partial \varepsilon}{\partial T}\right)_P - \varepsilon\left(\frac{\partial V}{\partial T}\right)_P}{V^2} = \gamma\frac{C_V}{V} - \gamma\frac{\varepsilon}{V^2}\left(\frac{\partial V}{\partial T}\right)_P \tag{7}$$

Here, K is the bulk modulus. According to the Grüneisen law, thermal

Table 1
The work of separation and interface distance of AlN(0001)/Ti(0001) at different temperatures.

	0 K	300 K	500 K	700 K
d_0, Å	2.24	2.29	2.31	2.3
W_{sep}, J/m^2	3.45	3.34	2.62	2.39

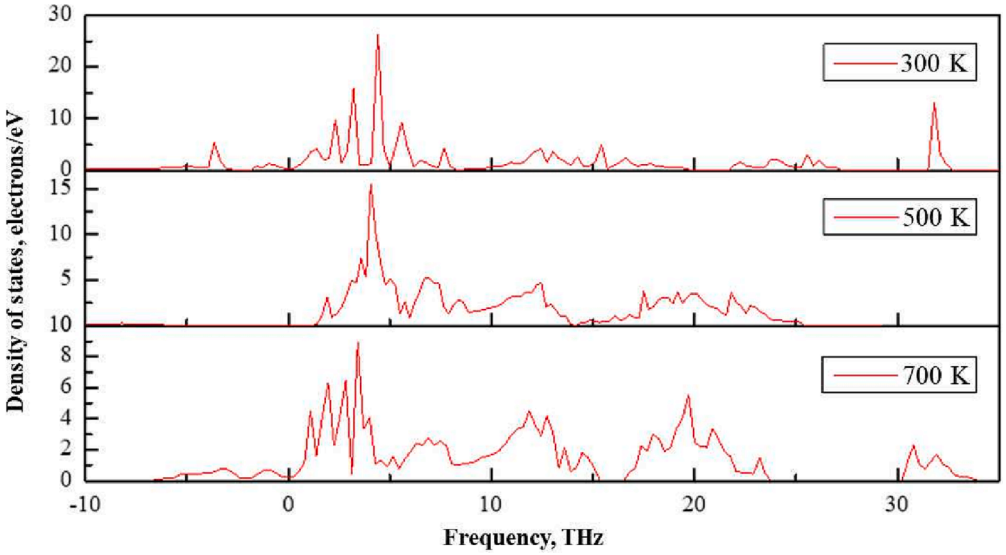

Fig. 4. Phonon density of states for the AlN/Ti interface at 300 K, 500 K, and 700 K.

expansion is proportional to the heat capacity at constant volume:

$$\alpha = \frac{\gamma}{VK} C_V \tag{8}$$

The elastic coefficients at different temperatures were determined using the first-principles strain–stress relationships method implemented by Milman [22]. Both positive and negative strains were applied for each strain component, with a maximum strain of 0.2%. The convergence criteria for atomic internal freedom optimization were selected as differences in the total energy within the 0.002 eV/Å Hellmann-Feynman force, and maximum ionic displacement within 1.104 Å. The bulk modulus B and shear modulus G were calculated from the compliance tensor by the Voigt-Reuss-Hill approximation.

3.3. Temperature-dependent anisotropic mechanical properties

To address the complicate mechanical response of AlN/Ti interface suffering external stress, the effective elastic behavior of this heterogeneous interface should be characterized. Evaluating the interfaces features between two phases with different elastic moduli have been vastly discussed by continuum mechanics. Continuum micromechanics theory was found on Eshelby's elasticity solution proposed the nonclassical stress–strain relationship featuring surface and/or interface effect [30,31]. It not only depends on intrinsic with lattice structure but also various with orientation and in-plane symmetries [32]. Zhang study shows interface bonding state such as localization of electron distribution also enhances on the interface elastic moduli. [33]. Developed on

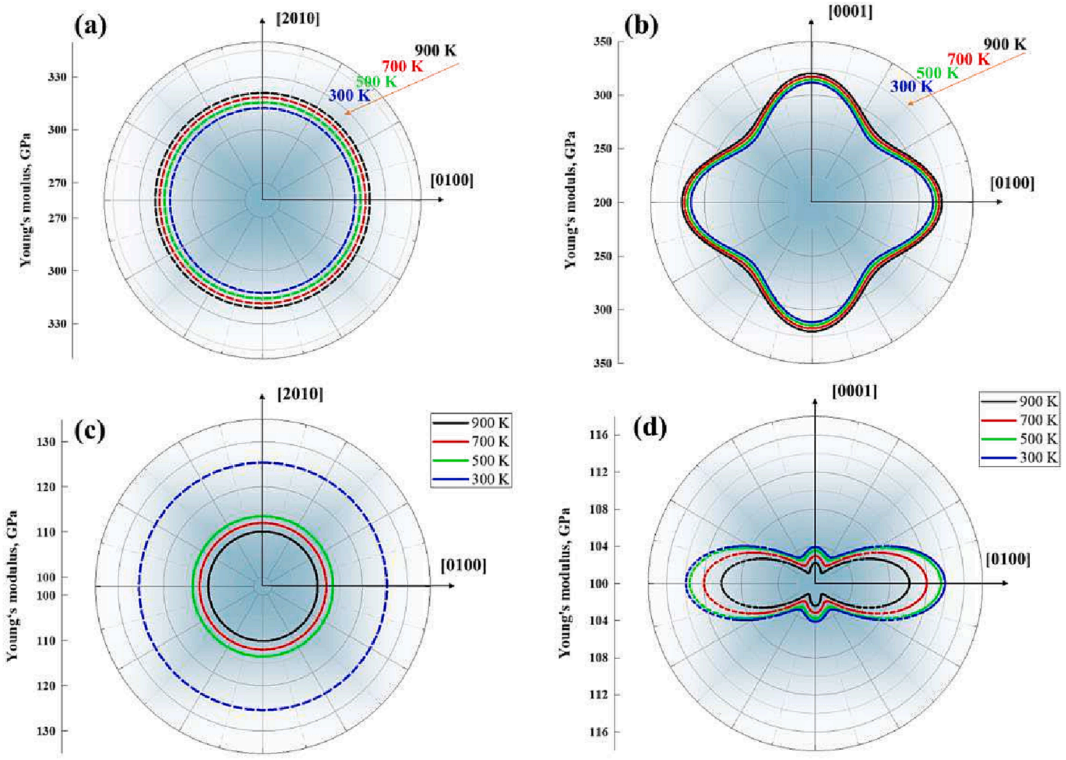

Fig. 5. Temperature-dependent Young's modulus: (a) AlN(0001); (b) AlN(1000); (c) Ti(0001); (d) Ti(1000).

our previous research on the AlN (0001)/Ti (0001) interface, higher Wsep and shorter d0 compared to other interface model states the stable structure. It is widely observed that elastic anisotropy of crystal structure caused disastrous engineering damage by initialing micro-defects and micro-voids. Therefore, it is essential to investigate the anisotropic mechanical properties at high temperatures to prevent thermal shock and stress. Direction-dependent Young's modulus E for hexagonal structure is defined as:

$$\frac{1}{E} = S_{11}\left(1 - g_3{}^2\right)^2 + S_{33}g_3{}^4 + (2S_{13} + 2S_{44})g_3{}^2\left(1 - g_3{}^2\right)^2 \quad (9)$$

Here, g_3 are the directional cosines of the angles with the c-axis. According to Eq. (9), Young's modulus is symmetric with the c-axis. For hexagonal crystal structure, thermal and direction-dependent Young's modulus of the most common {0001} and $\{10\bar{1}0\}$ crystallographic planes is shown in Fig. 5. The anisotropy factor $A_E = E_{MAX}/E_{MIN}$ decreased from 1.298, 1.296, and 1.295 to 1.294 at 300 K, 500 K, 700 K, and up to 900 K, respectively. The anisotropy factor of Ti decreased as temperature increased. As for the AlN, the anisotropy factor remains constant from 300 K to 900 K, varying from 1.202 to 1.203. The negligible increase in the anisotropy matches with the other hexagonal structures of high-temperature ceramics.

In addition, hexagonal structures often suffer from a lack of slip systems. Thus, shear modulus directionality strongly affects the shear behavior with the trend of the slip transfer from the basal (0001) plane to the prismatic $(10\bar{1}0)$ plane. To establish a certain slip plane, two given slip vectors have been set and polar plots constructed at different temperatures directly show the anisotropy in various directions. Three-dimensional shear modulus in all directions reflects the c-axis symmetry. The directionality of AlN (0001) has been projected and illustrated as the polar plots in Fig. 6.

4. Conclusions

The first-principles study of interfacial structures is presented, and thermodynamic and mechanical properties of the interface between AlN and Ti with different orientations were studied using the plane-wave pseudopotential method. The volume-dependent Helmholtz free energy, phonon density of states, Young's modulus, and shear modulus were investigated. The electronic properties and hybridization of the Ti-spd and N-p were discussed using the density of states. The orbital hybridization between N and Ti atoms in AlN(0001)/Ti(0001) interface shows strong thermal stability. Good thermal stability of the interfacial structure was found by the calculation of the work of separation, distance, and thermal volume expansion. The interfacial distance changed by 2.68% compared to the ground state. The decrease in the work of separation is in agreement with other metal/ceramic interfaces. The anisotropic Young's modulus and shear modulus were also calculated at elevated temperatures. The anisotropy factor of elastic modulus for AlN and Ti is 1.29 and 1.2 at elevated temperatures. The hexagonal crystal exhibits isotropic shear modulus in the basal (0001) plane as the elastic modulus. While on the $(1\bar{1}01)$ plane, the smallest shear modulus is along the [0001] direction, and the anisotropic factor is 1.09. The shear modulus and elastic modulus of AlN and Ti investigated from 300 K to 900 K show the same trend on their $(1\bar{1}01)$ plane. The thermal stability of the metal-ceramic interface sheds a light on its industrial applications in novel high-power microelectronic devices.

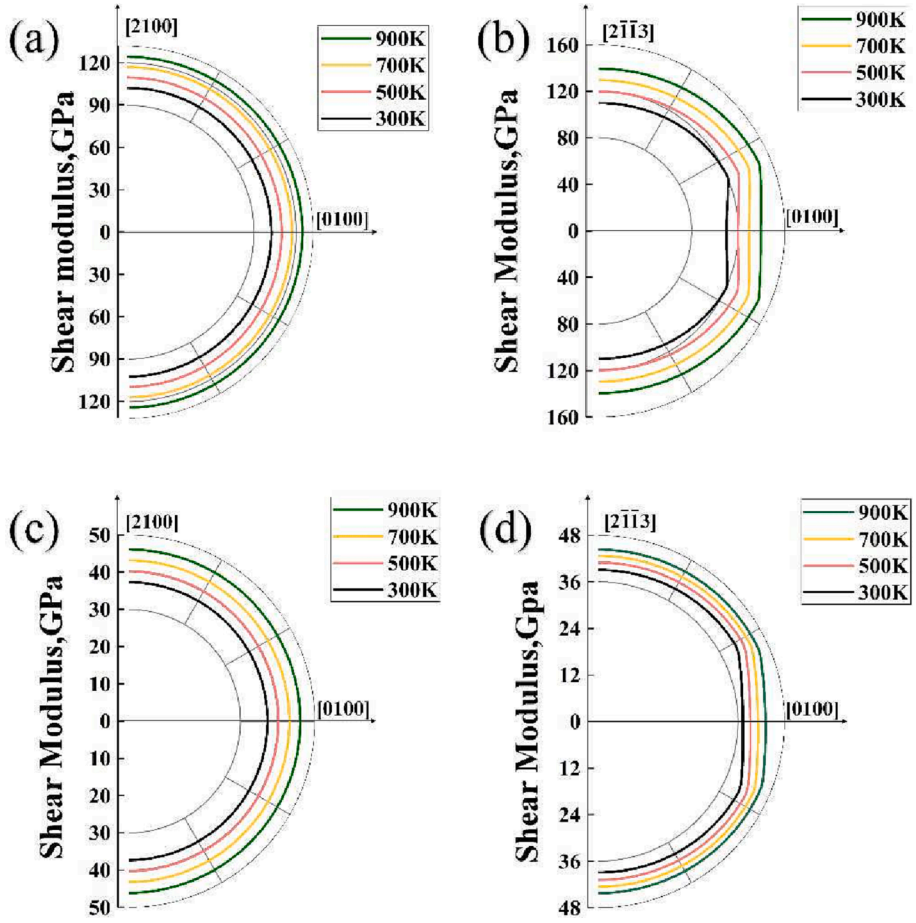

Fig. 6. Anisotropic Shear modulus at various temperatures: (a) AlN(0001); (b) AlN(1$\bar{1}$01); (c) Ti(0001); (d) Ti(1$\bar{1}$01).

CRediT authorship contribution statement

Lei Li: Visualization, Investigation. **Xueyan Yan:** Writing – original draft, Software, Data curation. **Bingzheng Yang:** Conceptualization, Methodology, Software, Data curation. **Sen Yang:** Writing – review & editing. **Alex A. Volinsky:** Writing – review & editing. **Xiaolu Pang:** Supervision.

Declaration of Competing Interest

The authors declare that they have no known competing financial interests or personal relationships that could have appeared to influence the work reported in this paper.

Data availability

No data was used for the research described in the article.

Acknowledgments

This work was supported by the National Natural Science Foundation of China (U21A2044, 52272057, 52001022), and the Science Center for Gas Turbine Project (P2021-A-IV-002-001, P2022-B-IV-008-001).

References

[1] A.J. Nozik, M.C. Beard, J.M. Luther, M. Law, R.J. Ellingson, J.C. Johnson, Semiconductor quantum dots and quantum dot arrays and applications of multiple exciton generation to third-generation photovoltaic solar cells, Chem. Rev. 110 (11) (2010) 6873–6890.
[2] RU H, WEI V, JIANG T, et al. Direct plated copper technology for high brightness LED packaging; proceedings of the 2011 6th International Microsystems, Packaging, Assembly and Circuits Technology Conference (IMPACT), F 19-21 Oct. 2011, 2011 [C].
[3] R. Khazaka, L. Mendizabal, D. Henry, R. Hanna, Survey of high-temperature reliability of power electronics packaging components, IEEE Trans. Power Electron. 30 (5) (2015) 2456–2464.
[4] LIN C H, HUANG P S, TSAI M Y, et al. Mechanical design and analysis of direct plated copper film on AlN substrates for thermal reliability in high power module applications; proceedings of the 2015 International Conference on Electronics Packaging and iMAPS All Asia Conference (ICEP-IAAC), F 14-17 April 2015, 2015 [C].
[5] M.Y. Tsai, C.H. Lin, K.F. Chuang, Y.H. Chang, C.T. Wu, S.C. Hu, Failure and stress analysis of through-aluminum-nitride-via substrates during thermal reliability tests for high power LED applications, Microelectron. Reliab. 67 (2016) 120–128.
[6] X.-F. Diao, Y.-L. Tang, D.-Y. Xiong, P.-R. Wang, L.-k. Gao, T.-y. Tang, X.-N. Wei, H.-R. Zhang, Xu-Pu wu, S.-T. Ji, Study on the properties of perovskite materials under light and different temperatures and electric fields based on DFT, RSC Adv. 10 (35) (2020) 20960–20971.
[7] B. Wang, K. Xiong, Z. Sun, W. Li, C. Jin, S. Zhang, L. Guo, Y. Mao, A DFT study on the crystal stability, mechanical, electronic and thermodynamic properties of Ir3Nb under high pressure and temperature, J. Phys. Chem. Solid 161 (2022) 110481.
[8] H. Yu, M. Bahadori, G.B. Thompson, C.R. Weinberger, Understanding dislocation slip in stoichiometric rocksalt transition metal carbides and nitrides, J. Mater. Sci. 52 (11) (2017) 6235–6248.
[9] X. Cai, Y. Luo, Adhesive properties study on the interfaces of AlN and metal of Pd, Ag and Cu, Sci. China Technol. Sci. 54 (1) (2011) 11–14.
[10] Y. Tao, G. Ke, Y. Xie, Y. Chen, S. Shi, H. Guo, Adhesion strength and nucleation thermodynamics of four metals (Al, Cu, Ti, Zr) on AlN substrates, Appl. Surf. Sci. 357 (2015) 8–13.
[11] S. Zhang, W. Jin, H. Yang, K. Gao, X. Pang, L. Yan, A.A. Volinsky, Comparative study of Ti and Cr adhesion to the AlN ceramic: experiments and calculations, Appl. Surf. Sci. 457 (2018) 856–862.
[12] H. Tanie, K. Nakane, Y. Urata, M. Tsuda, N. Ohno, Warpage variations of Si/solder/OFHC-Cu layered plates subjected to cyclic thermal loading, Microelectron. Reliab. 51 (9-11) (2011) 1840–1844.
[13] S. Pietranico, S. Pommier, S. Lefebvre, Z. Khatir, S. Bontemps, Characterisation of power modules ceramic substrates for reliability aspects, Microelectron. Reliab. 49 (9-11) (2009) 1260–1266.
[14] Y. Zhou, L. Xu, S. Liu, Optimization for warpage and residual stress due to reflow process in IGBT modules based on pre-warped substrate, Microelectron. Eng. 136 (2015) 63–70.
[15] S. Zhang, L. Yan, K. Gao, H. Yang, L. Yang, Y. Wang, X. Wan, Thermal ratchetting effect of AMB-AlN ceramic substrate: experiments and calculations, Ceram. Int. 45 (12) (2019) 14669–14674.
[16] W. Jin, L. Li, S. Zhang, H. Yang, K. Gao, X. Pang, A.A. Volinsky, First principles calculations of interfacial properties and electronic structure of the AlN(0 interface, Chem. Phys. Lett. 713 (2018) 153–159.
[17] G. Kresse, D. Joubert, From ultrasoft pseudopotentials to the projector augmented-wave method, Phys. Rev. B 59 (3) (1999) 1758–1775.
[18] G. Kresse, J. Furthmüller, Efficient iterative schemes for ab initio total-energy calculations using a plane-wave basis set, Phys. Rev. B 54 (16) (1996) 11169–11186.
[19] P.E. Blöchl, Projector augmented-wave method, Phys. Rev. B 50 (24) (1994) 17953–17979.
[20] J.P. Perdew, K. Burke, M. Ernzerhof, Generalized gradient approximation made simple, Phys. Rev. Lett. 77 (18) (1996) 3865–3868.
[21] P. Vinet, J.H. Rose, J. Ferrante, J.R. Smith, Universal features of the equation of state of solids, J. Phys. Condens. Matter 1 (11) (1989) 1941–1963.
[22] V. Milman, M.C. Warren, Elasticity of hexagonal BeO, J. Phys. Condens. Matter 13 (2) (2001) 241–251.
[23] R. Hill, The elastic behaviour of a crystalline aggregate, Proc. Phys. Soc. A 65 (5) (1952) 349–354.
[24] A. Reuss, Berechnung der Fließgrenze von Mischkristallen auf Grund der Plastizitätsbedingung für Einkristalle, ZAMM - Journal of Applied Mathematics and Mechanics / Zeitschrift für Angewandte Mathematik und Mechanik 9 (1) (1929) 49–58.
[25] A.J. Wang, S.L. Shang, Y. Du, Y. Kong, L.J. Zhang, L. Chen, D.D. Zhao, Z.K. Liu, Structural and elastic properties of cubic and hexagonal TiN and AlN from first-principles calculations, Comput. Mater. Sci 48 (3) (2010) 705–709.
[26] R.F. Zhang, S. Veprek, Metastable phases and spinodal decomposition in Ti1−xAlxN system studied by ab initio and thermodynamic modeling, a comparison with the TiN–Si3N4 system, Mater. Sci. Eng. A 448 (1) (2007) 111–119.
[27] H. Schulz, K.H. Thiemann, Crystal structure refinement of AlN and GaN, Solid State Commun. 23 (11) (1977) 815–819.
[28] A.Y. Kuksin, A.S. Rokhmanenkov, V.V. Stegailov, Atomic positions and diffusion paths of h and he in the α-Ti lattice, Phys. Solid State 55 (2) (2013) 367–372.
[29] L.-C. Xu, R.-Z. Wang, X. Yang, H. Yan, Thermal expansions in wurtzite AlN, GaN, and InN: First-principle phonon calculations, J. Appl. Phys. 110 (4) (2011) 043528.
[30] Y. Benveniste, A general interface model for a three-dimensional curved thin anisotropic interphase between two anisotropic media, J. Mech. Phys. Solids 54 (4) (2006) 708–734.
[31] K. Bertoldi, D. Bigoni, W.J. Drugan, Structural interfaces in linear elasticity. Part I: Nonlocality and gradient approximations, J. Mech. Phys. Solids 55 (1) (2007) 1–34.
[32] C. Mi, S. Jun, D.A. Kouris, S.Y. Kim, Atomistic calculations of interface elastic properties in noncoherent metallic bilayers, Phys. Rev. B 77 (7) (2008), 075425.
[33] T. Zhang, Y. Chen, H. Xie, N. Zhao, C. Shi, C. He, E. Liu, Regulation of the interface binding and elastic properties of sic/ti via doping-induced electronic localization, Physica Status Solidi (b) 257 (1) (2020) 1900163.